



HAL
open science

Validation of calibration strategies for macroscopic traffic flow models on synthetic data

Alexandra Würth, Mickael Binois, Paola Goatin

► **To cite this version:**

Alexandra Würth, Mickael Binois, Paola Goatin. Validation of calibration strategies for macroscopic traffic flow models on synthetic data. 8th International Conference on Models and Technologies for Intelligent Transportation Systems (MT-ITS 2023), Jun 2023, Saint-Laurent-Du-Var, France. hal-04197769

HAL Id: hal-04197769

<https://hal.science/hal-04197769v1>

Submitted on 6 Sep 2023

HAL is a multi-disciplinary open access archive for the deposit and dissemination of scientific research documents, whether they are published or not. The documents may come from teaching and research institutions in France or abroad, or from public or private research centers.

L'archive ouverte pluridisciplinaire **HAL**, est destinée au dépôt et à la diffusion de documents scientifiques de niveau recherche, publiés ou non, émanant des établissements d'enseignement et de recherche français ou étrangers, des laboratoires publics ou privés.

Validation of calibration strategies for macroscopic traffic flow models on synthetic data

Alexandra Würth
Université Côte d'Azur
Inria, CNRS, LJAD
Sophia Antipolis, France
alexandra.wuerth@inria.fr

Mickaël Binois
Université Côte d'Azur
Inria, CNRS, LJAD
Sophia Antipolis, France
mickael.binois@inria.fr

Paola Goatin
Université Côte d'Azur
Inria, CNRS, LJAD
Sophia Antipolis, France
paola.goatin@inria.fr

Abstract—We analyze two calibration approaches for parameter identification and traffic speed reconstruction in macroscopic traffic flow models. We consider artificially created noisy loop detector data as our field measurements. Due to the knowledge of the ground truth calibration parameter, we can give a sound assessment with respect to the performance of the considered methods. Our analysis shows that, in the proposed setting, the first order traffic flow model together with the proposed Kennedy O'Hagan approach performs better in reconstructing the speed traffic quantity than the other approaches.

Key words: Macroscopic traffic flow models; synthetic loop detector data; Gaussian process modeling; parameter estimation; optimization.

I. INTRODUCTION

Macroscopic traffic flow models, consisting in hyperbolic partial differential equations based on the mass conservation principle, describe the spatio-temporal evolution of traffic aggregate quantities such as density and mean velocity on road networks. Since they involve few parameters and they are computationally less expensive, they are often a preferred choice over other models (such as microscopic ones). Nevertheless, parameter calibration remains a challenging task due to model limitations and data noise.

In this work, we focus on the comparison of two different calibration approaches applied to first order models, consisting in the sole mass conservation equation, and second order ones, including a second equation accounting for speed evolution. The models are based on a speed function including unknown parameters. Typically, the model parameters are calibrated by fitting the so-called fundamental diagram, i.e., the density-flow or density-speed mapping described by the model flux function (see e.g. [1], [2]). However, data noise and congested traffic situations make the parameter identification process difficult to deal with (see e.g. [3]). In this paper, we consider the following alternative approaches. One consists in minimizing

This work has been supported by the French government, through the 3IA Côte d'Azur Investments in the Future project managed by the National Research Agency (ANR) with the reference number ANR-19-P3IA-0002.

the L^2 -error between the simulation output and the (synthetic) data [4]–[6]. The other one was proposed in [3] and follows [7]: it introduces a bias term to better account for possible discrepancies between the mathematical models and reality. This generic framework has been applied in a variety of fields, ranging from physics [8] to engineering [9] or biology [10].

To better assess the performances of the proposed approaches and the considered models, we employ average loop detector data constructed by numerical simulations. By testing and comparing the performances of two calibration methods, we aim at providing a benchmark for applying the selected approaches in real world situations.

The article is organized as follows. In Section II, we introduce the considered discrete traffic modeling framework and we detail the numerical scheme used to produce the synthetic data in Section III and to run the calibration algorithms presented in Section IV. Finally, the optimization results are discussed in Section V and a conclusion is made in Section VI. We remark that throughout the paper, we will follow notations from [3].

II. DISCRETE MACROSCOPIC TRAFFIC FLOW MODELS

We consider the following discretization in space and time of the initial boundary value problem for the Generic Second Order Model (GSOM) [11] on a road stretch including on- and off-ramps. Given a discretization $\{x_0, \dots, x_M\}$ of the spatial interval $]x_{in}, x_{out}[$ (with $x_0 = x_{in}$ and $x_M = x_{out}$ and including ramp locations), we set the cell sizes $\Delta x_j := x_j - x_{j-1}$ for $j = 1, \dots, M$, and a time step Δt satisfying a suitable stability condition to be specified later. Denoting by ρ_j^n and w_j^n respectively the traffic density, the Lagrangian vehicle property in section j at time $n\Delta t$, the traffic speed is given by $v_j^n = \mathcal{V}(\rho_j^n, w_j^n)$, where the speed function \mathcal{V} satisfies: $\mathcal{V}(\rho, w) \geq 0$, $\mathcal{V}(0, w) = w$, $2\mathcal{V}_\rho(\rho, w) + \rho\mathcal{V}_{\rho\rho}(\rho, w) < 0$ for $w > 0$ and $\mathcal{V}_w(\rho, w) > 0$. As a consequence, the flow function $\rho \mapsto Q(\rho, w) := \rho\mathcal{V}(\rho, w)$ is strictly concave for $w > 0$ and we denote by $\rho_{cr}(w)$ the point where it achieves its maximum. Moreover, we denote by $r_j^{\rho, n}$ and $s_j^{\rho, n}$ respectively the on-ramp and off-ramp fluxes at x_j and $n\Delta t$.

Setting $\mathbf{U}_j^n := (\rho_j^n, \rho_j^n w_j^n)^\top$, the discrete GSOM equations read for $j \in \{1, \dots, M-1\}$:

if $r_j^{\rho, n} \geq 0$ and $s_j^{\rho, n} = 0$ (and $r_{j-1}^{\rho, n} = s_{j-1}^{\rho, n} = 0$):

$$\begin{cases} \mathbf{U}_j^{n+1} = \mathbf{U}_j^n - \frac{\Delta t}{\Delta x_j} \left[\min \left\{ \mathbf{D}(\mathbf{U}_j^n), \max \{ P_j \mathbf{S}(\mathbf{U}_{j+1}^n; w_j^n), \right. \right. \\ \left. \left. \mathbf{S}(\mathbf{U}_{j+1}^n; w_j^n) - \mathbf{r}_j^n \right\} - \mathbf{F}_{j-1}^n \right], \\ \mathbf{U}_{j+1}^{n+1} = \mathbf{U}_{j+1}^n - \frac{\Delta t}{\Delta x_{j+1}} \left[\mathbf{F}_{j+1}^n - \min \{ \mathbf{D}(\mathbf{U}_j^n) + \mathbf{r}_j^n, \mathbf{S}(\mathbf{U}_{j+1}^n; w_j^n) \} \right]; \end{cases}$$

if $s_j^{\rho, n} > 0$ and $r_j^{\rho, n} = 0$ (and $r_{j-1}^{\rho, n} = s_{j-1}^{\rho, n} = 0$):

$$\begin{cases} \mathbf{U}_j^{n+1} = \mathbf{U}_j^n - \frac{\Delta t}{\Delta x_j} \left[\left(\min \left\{ \max \{ \mathbf{D}(\mathbf{U}_j^n) - \mathbf{s}_j^n, 0 \}, \right. \right. \right. \\ \left. \left. \left. \mathbf{S}(\mathbf{U}_{j+1}^n; w_j^n) \right\} + \min \{ \mathbf{D}(\mathbf{U}_j^n), \mathbf{s}_j^n \} \right) - \mathbf{F}_{j-1}^n \right], \\ \mathbf{U}_{j+1}^{n+1} = \mathbf{U}_{j+1}^n - \frac{\Delta t}{\Delta x_{j+1}} \left[\mathbf{F}_{j+1}^n - \min \left\{ \max \{ \mathbf{D}(\mathbf{U}_j^n) - \mathbf{s}_j^n, 0 \}, \right. \right. \\ \left. \left. \mathbf{S}(\mathbf{U}_{j+1}^n; w_j^n) \right\} \right], \end{cases}$$

where $\mathbf{r}_j^n := (r_j^{\rho, n}, w_j^n r_j^{\rho, n})^\top$, $\mathbf{s}_j^n := (s_j^{\rho, n}, w_j^n s_j^{\rho, n})^\top$ and $P_j \in [0, 1]$ are the priority parameters at on-ramps. Moreover, the initial and boundary data are approximated by piecewise constant functions \mathbf{U}_j^0 , \mathbf{U}_0^n and \mathbf{U}_M^n . We remark that the discretization is chosen in a way such that we cannot have two ramps on subsequent cell-interfaces.

The demand and supply functions in the above scheme are defined by $\mathbf{D}(\mathbf{U}_j) = (D^\rho(\mathbf{U}_j), w_j D^\rho(\mathbf{U}_j))^\top$ and $\mathbf{S}(\mathbf{U}_{j+1}) = (S^\rho(\mathbf{U}_{j+1}; w_j), w_j S^\rho(\mathbf{U}_{j+1}; w_j))^\top$ with

$$D^\rho(\mathbf{U}_j) = \begin{cases} Q(\rho_j, w_j) & \text{if } \rho_j \leq \rho_{cr}(w_j), \\ Q(\rho_{cr}(w_j), w_j) & \text{if } \rho_j > \rho_{cr}(w_j), \end{cases}$$

$$S^\rho(\mathbf{U}_{j+1}, w_j) = \begin{cases} Q(\rho_{cr}(w_j), w_j) & \text{if } \rho_{j+1/2} \leq \rho_{cr}(w_j), \\ Q(\rho_{j+1/2}, w_j) & \text{if } \rho_{j+1/2} > \rho_{cr}(w_j), \end{cases}$$

and where $\rho_{j+1/2}$ is the density of the intermediate state in the solution of the Riemann problem corresponding to (ρ_j, w_j) and (ρ_{j+1}, w_{j+1}) , implicitly defined by $\mathcal{V}(\rho_{j+1/2}, w_j) = \mathcal{V}(\rho_{j+1}, w_{j+1})$ if $\mathcal{V}(\rho_{j+1}, w_{j+1}) \leq w_j$ and by $\rho_{j+1/2} = 0$ if $\mathcal{V}(\rho_{j+1}, w_{j+1}) > w_j$ [12].

Finally, to compute $\mathbf{F}_j^n = (F_j^{\rho, n}, w_j^n F_j^{\rho, n})^\top$, we set

$$F_j^{\rho, n} = \min \left\{ D^\rho(\mathbf{U}_j^n), S^\rho(\mathbf{U}_{j+1}^n; w_j^n) \right\}. \quad (\text{II.1})$$

Note that, taking $w_j^n = \text{const}$ in the above equations, we recover the first order Lighthill-Whitham-Richards (LWR) model [13], [14] in its CTM version [15].

In the following, we consider the speed function

$$\mathcal{V}(\rho, w) = w \left(1 - \exp \left(\frac{C}{V} \left(1 - \frac{R}{\rho} \right) \right) \right), \quad (\text{II.2})$$

proposed by Newell-Franklin [16], [17]. Thus, the Courant-Friedrichs-Lewy (CFL) stability condition reads as

$$\Delta t \leq \frac{\min_j \Delta x_j}{\max\{C, V\}} \quad (\text{II.3})$$

and the parameters to be identified are $\theta = (V, C, R)$, where $V > 0$ is the maximal speed, $R > 0$ is the maximal density and $C > 0$ is the wave propagation speed in congestion. Again, the LWR model is obtained by fixing $w = V$ in (II.2).

III. SYNTHETIC DATA CONSTRUCTION

We consider a road stretch of $L = 4.85$ km long accounting for 8 loop detectors, 3 off-ramps and 2 on-ramps. The road is divided into 11 intervals (see Figure 1), each containing 30 mesh points (i.e. $M = 330$).

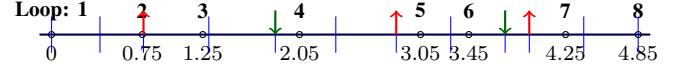


Fig. 1: Schematic representation of the considered road stretch. Blue vertical lines represent the coarse segmentation. The red (resp. green) arrows mark off- (resp. on-) ramp locations.

For the generation of the synthetic data set, we set

$$\theta^0 = (V^0, C^0, R^0) = (100, 20, 350)$$

and we consider a bell-shaped initial traffic density over $x \in [0, L]$:

$$\rho(0, x) = 0.92R \cdot \exp \left(-\frac{(x - \frac{L}{2})^2}{2 \cdot (0.1L)^2} \right),$$

and boundary data given by:

$$\rho(t, 0) = \rho(t, L) = 0.45R \cdot \sin \left(\frac{4\pi}{3} \left(t - \frac{3}{8} \right) \right) + 0.05R$$

(see Figure 2). The artificial ramp flows are based on the

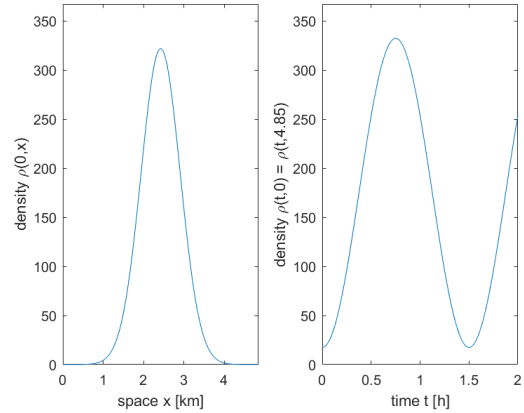


Fig. 2: Illustration of initial (left figure) and boundary data (right figure).

functions:

$$q_i^{ramp}(t) = a_i R \cdot \sin \left(\frac{2\pi}{b_i} (t - c_i) \right) + d_i R,$$

where $a_i, b_i, c_i, d_i \in]0, 1.5[$, $i \in \{1, \dots, 5\}$, are chosen arbitrarily. The priority on-ramp parameters P_j are all set to $5/6$ in the numerical scheme.

Data are generated by the following procedure. We run a simulation, taking $w = V$, $\theta = \theta^0$ and data $\rho(t, 0) = \rho(t, L)$ and $q_i^{ramp}(t)$, $i \in \{1, \dots, 5\}$ at $t \in \{\Delta t, 2\Delta t, \dots, 2\}$ with $\Delta t = 6 \cdot 10^{-5}$ hr and $\rho(0, x)$ at $x \in \{\frac{x_1 - x_0}{2} + x_0, \frac{x_2 - x_1}{2} + x_1, \dots, \frac{x_M - x_{M-1}}{2} + x_{M-1}\}$. We remark that the simulation output is given in terms of the density (and additionally speed in the GSOM model). The corresponding speed and flow values are generated by means of (II.2).

Then, in order to create a more realistic traffic situation, we add a discrepancy term to the simulated quantities (density, speed and flow), denoted by y_{sim} . Since the amount of the discrepancy is unknown, we analyze three different scenarios: no, low or high discrepancy. Thus, the ground truth traffic quantities are given by

$$y^P(t, x) := y_{sim}(t, x) + \tau \max\{y_{sim}(t, x)\} \cdot \sin(t + x) \quad (\text{III.1})$$

where $\tau \in \{0, 0.02, 0.1\}$ (negative values are replaced by zero). Figure 3 visualizes the speed reference traffic situation in the case of a low bias ($\tau = 0.02$). We emphasize that the selected time window (2 hours) accounts for both congestion (red colored velocities) and free flow (green colored velocities) phases. The rush hour begins after about 25 minutes, spilling back from the downstream boundary, and dissipates after approximately 100 minutes. Moreover, we also remark the effect of the ramp flows, which is shown by the horizontal lines corresponding to the ramp positions.

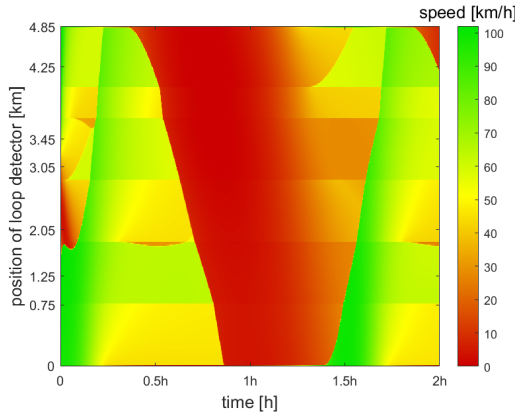


Fig. 3: Space-time speed visualization for the simulated scenario, $\tau = 0.02$.

In general, the field data y^F measured by loop detectors are noisy averages of the real data. Thus, we define y^F by taking 6 minute averages of the ground truth y^P , denoted by \bar{y}^P , and by adding a normal distributed random variable, i.e.

$$y^F = \bar{y}^P + s\bar{y}^P \mathcal{N}(0, 1),$$

where we set $s = 0.15$. Again, negative values are set to zero. The synthetic ramp flows are obtained by the same procedure. To emphasize the difference between \bar{y}^P and y^F , Figure 4 shows the constructed average flow-density and speed-density pairs together with the speed function (II.2) ($w = V$, $\theta = \theta^0$).

If $\tau = 0$, the reference data points \bar{y}^P lie closely around the curve. Coherently, if we consider a high discrepancy ($\tau = 0.1$), the data \bar{y}^P are further away from the red line. In both cases the noisy data y^F are more widely spread but they are still following the shape of the curve.

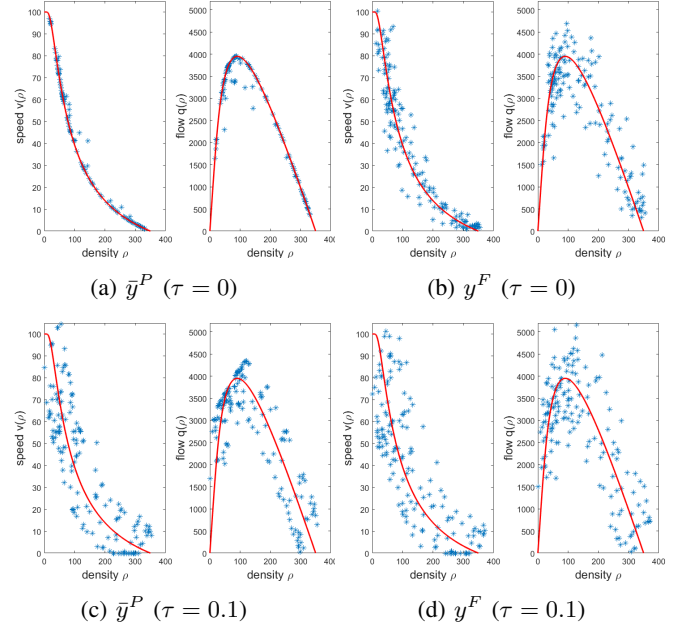


Fig. 4: Fundamental diagrams for 6 minute average reference (\bar{y}^P) and noisy data (y^F), $\tau \in \{0, 0.1\}$.

To conclude this section, we also plot the density profiles corresponding to \bar{y}^P and y^F for each loop detector in Figure 5. The noisy averaged data clearly follow the evolution of the reference data. However, in higher density regions, the deviation is more strongly present due to the multiplicative noise ($s\bar{y}^P$) in the field data construction.

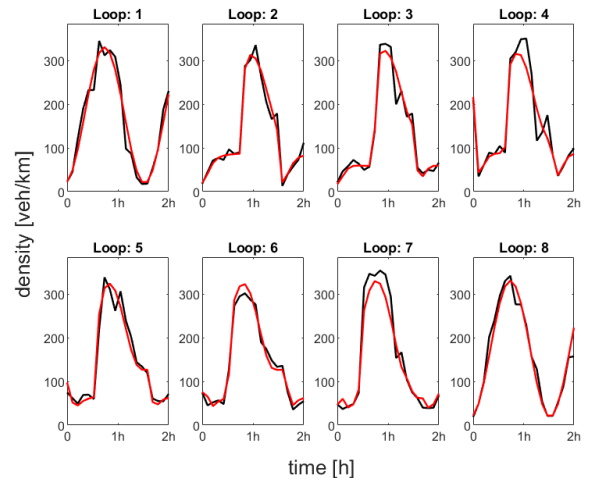


Fig. 5: Density profiles for 6 minute average real (\bar{y}^P , in red) and noisy data (y^F , in black), $\tau = 0$.

Remark 1. In order to create a realistic traffic environment, the choice of our artificial traffic scenario is motivated by the RTMC data set [18] provided by the Minnesota Department of Transportation (MnDOT): the distances between the main loop (resp. ramp) detectors coincide with those of the detectors S54, S1706, S56, S57, S1707, S59, S60, S61 (resp. 129, 130, 169, 170, 171) on the highway I-35W.

IV. CALIBRATION APPROACHES

In this section, we describe two calibration approaches to identify the parameter θ which is used to generate the simulated (sim.) traffic data y^M .

For constructing the simulated data, we extract the initial and boundary data from y^F . These data serve as inputs for the numerical simulations. Then, the calibration is done by standard \mathbf{L}^2 -optimization (see Definition 1) or the KOH-optimization (see Definition 2) introduced in [7], [8].

Some notation are needed before defining the two calibration approaches: given a set of observations of the field data $(y^F((t_1, x_1), \dots, (t_N, x_N)))$ at N observation points $\mathcal{X}_N = ((t_1, x_1), \dots, (t_N, x_N))$, we define the observed (noisy) bias at observation point $i \in \{1, \dots, N\}$ as

$$b_i(\theta) = y^F(t_i, x_i) - y^M(t_i, x_i, \theta)$$

and the set of observed biases \mathbf{b}_N by

$$\mathbf{b}_N(\theta) = y^F(\mathcal{X}_N) - y^M(\mathcal{X}_N, \theta).$$

Definition 1. The \mathbf{L}^2 -optimization consists in minimizing the least square cost function C given by

$$C(\theta) = \sum_{i=1}^N |b_i(\theta)|^2.$$

Thus, the optimal parameter θ^* is given by

$$\theta^* = \underset{\theta}{\operatorname{argmin}} C(\theta).$$

Definition 2. The KOH-optimization relies on a Gaussian process (GP) for estimating the bias term, which amounts to consider \mathbf{b}_N as a realization of a multivariate normal distribution:

$$\mathbf{b}_N \sim \mathcal{N}(\mathbf{0}_N, \sigma^2(\mathbf{C}_N(l_1, l_2) + g\mathbf{I}_N)).$$

The optimal parameters are those maximizing the concentrated log-likelihood function:

$$\max_{l_1, l_2, g, \theta} \log \tilde{\mathcal{L}}(l_1, l_2, g, \theta)$$

with

$$\begin{aligned} \log \tilde{\mathcal{L}}(l_1, l_2, g, \theta) = & -\frac{N}{2} \log 2\pi - \frac{N}{2} \log \hat{\sigma}^2(l_1, l_2, g, \theta) \\ & - \frac{1}{2} \log |\mathbf{C}_N(l_1, l_2) + g\mathbf{I}_N| - \frac{N}{2}, \end{aligned} \quad (\text{IV.1})$$

where the process variance is defined as

$$\hat{\sigma}^2(l_1, l_2, g, \theta) = \frac{\mathbf{b}_N(\theta)^\top (\mathbf{C}_N(l_1, l_2) + g\mathbf{I}_N)^{-1} \mathbf{b}_N(\theta)}{N}.$$

In Definition 2, \mathbf{C}_N denotes the correlation matrix between the observed biases \mathbf{b}_N . More precisely, the matrix entries of \mathbf{C}_N are given by the following positive definite function:

$$\begin{aligned} c((t, x), (t', x')) = & \quad (\text{IV.2}) \\ \frac{1}{\Delta t^2} \int_{t'}^{t'+\Delta t} \int_t^{t+\Delta t} \exp\left(-\frac{(t-t')^2}{l_1^2}\right) \cdot \exp\left(-\frac{(x-x')^2}{l_2^2}\right) ds ds'. \end{aligned}$$

The (hyper-)parameters l_1 and l_2 denote, respectively, the length-scales for the time and space variables and g accounts for unknown measurement noise in the bias.

Remark 2. The correlation function (IV.2) is obtained by integrating twice the commonly used Gaussian kernel. This is motivated by the fact that we consider averaged data. The idea is based on [19, Section 4.7].

Finally, in both approaches, we model the bias at \hat{n} new locations $\hat{\mathcal{X}}_{\hat{n}} = ((\hat{t}_1, \hat{x}_1), \dots, (\hat{t}_{\hat{n}}, \hat{x}_{\hat{n}}))$ by

$$\mathbf{b}(\hat{\mathcal{X}}_{\hat{n}}) | \mathbf{b}_N \sim \mathcal{N}(m_N(\hat{\mathcal{X}}_{\hat{n}}), s_N^2(\hat{\mathcal{X}}_{\hat{n}}, \hat{\mathcal{X}}_{\hat{n}})),$$

where

$$\begin{aligned} m_N(\hat{\mathcal{X}}_{\hat{n}}) &:= \mathbf{k}_N(\hat{\mathcal{X}}_{\hat{n}})^\top \mathbf{K}_N^{-1} \mathbf{b}_N, \\ s_N^2(\hat{\mathcal{X}}_{\hat{n}}, \hat{\mathcal{X}}_{\hat{n}}) &:= k(\hat{\mathcal{X}}_{\hat{n}}, \hat{\mathcal{X}}_{\hat{n}}) - \mathbf{k}_N(\hat{\mathcal{X}}_{\hat{n}})^\top \mathbf{K}_N^{-1} \mathbf{k}_N(\hat{\mathcal{X}}_{\hat{n}}), \end{aligned}$$

and

$$\begin{aligned} k(\cdot, \cdot) &:= \hat{\sigma}^2 c(\cdot, \cdot), \\ \mathbf{k}_N(\hat{\mathcal{X}}_{\hat{n}}) &:= (k(\hat{\mathcal{X}}_{\hat{n}}^{(j)}, \mathcal{X}_N^{(i)}))_{1 \leq j \leq \hat{n}, 1 \leq i \leq N}. \end{aligned}$$

We refer to [3], [7], [8] for more details on GP modeling.

Finally, the corrected calibrated simulated (corr. sim.) data, y_c^M , are computed by $y_c^M = y^M + m_N(\mathcal{X}_N)$. Possibly negative values are set to zero.

In the following, we will use the abbreviation M-A when considering model M (LWR or GSOM) and approach A (L2 or KOH).

A. Optimization specifications

In order to overcome the difficulty of precisely reconstructing the initial density condition from point-wise loop measurements, we run the traffic model through an initialization phase of 6 minutes (see [1]). Thus, the calibration of the parameters will be finally done on a 1 hour 54 minutes time slot.

Moreover, in the KOH approach, we apply a 2-step optimization procedure to separate the hyper- and calibration parameter computation. In the so-called *inner-level*, we maximize the concentrated log-likelihood function (IV.1) dependent on θ , thus obtaining the hyperparameters l_1, l_2, g . These hyperparameters are inserted again into (IV.1) which will be then maximized with respect to θ , giving the optimized

calibration parameter θ^* . We call the second step the *higher-level*. We observe that for the inner-level, it is sufficient to execute the local MATLAB optimization solver `fmincon`, since trying several choices of initial guesses leads to very similar optimization result. However, for the higher level, we observe a stronger dependence on the initial guess, hence we combine the global `pso` (particle swarm optimization) and `fmincon` solver (by setting the option `HybridFcn`) to reduce the probability of being stuck in a local minimum.

V. VALIDATION AND COMPARISON

In the following, we present and compare our results concerning the two calibration approaches introduced in Section IV. Our quantity of interest (y^i , $i \in \{P, F, M\}$) is the speed, since the final goal is to match the numerical simulation output y^M as good as possible with the synthetic traffic data y^F in order to do travel time prediction in future works. Thus, also the calibration is executed on the speed quantity.

In order to compare the predictive accuracy between the two calibration approaches and traffic flow models, we consider the error metric \mathbf{E} given by the root mean square error (RMSE) between the field data and the corrected calibrated simulated data:

$$\mathbf{E} = \sqrt{\frac{1}{N} \sum_{(t,x) \in (T,X)} |y^F(t,x) - y_c^M(t,x,\theta^*)|^2}$$

where (T, X) denotes the N (t, x) points where observations have been measured.

Table I compares the results between the above introduced calibration approaches and first and second order traffic models. The relative error with respect to the ground truth parameter θ^0 is indicated in brackets.

TABLE I: Optimization results for $\tau \in \{0, 0.02, 0.1\}$.

(a) LWR model.

	τ	\mathbf{E}	V	C	R
L2	0.00	7.3	96.3 (-3.7%)	18.4 (-7.9%)	379.5 (+8.4%)
	0.02	7.1	95.5 (-4.5%)	20.0 (+0.1%)	378.6 (+8.2%)
	0.10	7.9	88.1 (-11.9%)	27.3 (+36.7%)	372.1 (+6.3%)
KOH	0.00	7.3	95.1 (-5.0%)	18.4 (-7.8%)	378.2 (+8.0%)
	0.02	7.1	98.8 (-1.3%)	19.9 (-0.5%)	382.2 (+9.2%)
	0.10	6.2	92.7 (-7.3%)	25.2 (+26.0%)	373.3 (+6.7%)

(b) GSOM model.

	τ	\mathbf{E}	V	C	R
L2	0.00	7.9	93.1 (-6.9%)	20.4 (+2.1%)	353.4 (+1.0%)
	0.02	7.9	96.4 (-3.6%)	24.2 (+20.8%)	377.1 (+7.7%)
	0.10	9.6	92.0 (-8.0%)	21.6 (+8.2%)	439.1 (+25.5%)
KOH	0.00	5.9	116.8 (+16.0%)	27.1 (+3.05%)	356.8 (+1.9%)
	0.02	7.9	104.1 (+4.1%)	26.3 (+31.5%)	377.0 (+7.7%)
	0.10	8.2	76.3 (-23.7%)	34.9 (+74.7%)	447.0 (+27.7%)

The following analysis will differentiate between the results of the parameter reconstruction and error \mathbf{E} minimization.

First, we emphasize that none of the tests achieves to identify

the parameter exactly. However we observe different performances: starting by comparing the calibration approaches, we observe a similar reconstruction for the maximum density R values. The performance in the reconstruction of C and V is less clear in the LWR model, but strikingly better in the GSOM-L² approach. Next, looking at the two traffic flow models, we detect a clear outperformance of the GSOM model with respect to R in the case $\tau = 0$. However, increasing the bias leads to an obvious rise in R . This behaviour cannot be observed in the LWR model. Moreover, the V parameter is similarly or better reconstructed by the LWR model. For the C parameter, it is not possible to draw a conclusion, but we observe large outliers in the GSOM model even with low biased ($\tau = 0.02$) data. At this state, we can conclude that the parameter values vary more strongly for the GSOM model, thus the LWR model seems to be more stable in terms of parameter reconstruction. However, we point out that unreasonable parameters do not necessarily lead to bad estimations especially in high bias situations. This is due to a change in the real data y^P (see (III.1)), thus a different θ (from the ground truth θ^0) can be optimal for reconstructing y^F (or y^P).

Now, comparing the error \mathbf{E} , we observe a surprisingly good performance for the GSOM-KOH approach in the case $\tau = 0$, although the errors in the V and C parameters are high. Considering the speed profiles for y^F , y^M and y_c^M plotted in Figure 6, we observe that this result can be related to the very good reconstruction at the boundary loop detectors (loops 1 and 8). This is not surprising, since the GSOM includes the boundary speed as input data for the numerical scheme.

Additionally, by increasing the bias, we observe a better performance of the KOH approach compared to the L² one. This was expected, since the KOH approach should capture the bias contribution. Moreover, it is clearly visible that the LWR model outperforms the GSOM model, which deteriorates more strongly when the bias increases. We remark that the lowest error for each τ -value is highlighted in bold in Table I.

From the above analysis, we conclude that, assuming observation noise in the data, the ground truth parameters do not necessarily lead to the best reconstruction of the field data y^F . In fact, running our algorithm with $\theta = \theta^0$, we obtain $\mathbf{E} = 7.5$ ($\tau = 0$) (7.6 ($\tau = 0.02$) and 9.3 ($\tau = 0.1$)), which is worse than the corresponding errors in the LWR model in Table I.

Since we are interested in travel time predictions, we finally compare the RMSE (see Table II) between the corrected simulation and the averaged traffic data \bar{y}^P . Naturally, the higher the bias, the larger the error. We observe again that the LWR outperforms the GSOM model and the KOH beats the L² approach in increased bias situations (see values in bold). We emphasize again that in reality we do not have access to y^P (and thus \bar{y}^P) (due to measurement noise) therefore it is not possible to confirm this conclusion. However, the results of this paper can be seen as an indication of which approach leads more likely to the lowest RMSE for real traffic data.

Remark 3. We emphasize that although the second order

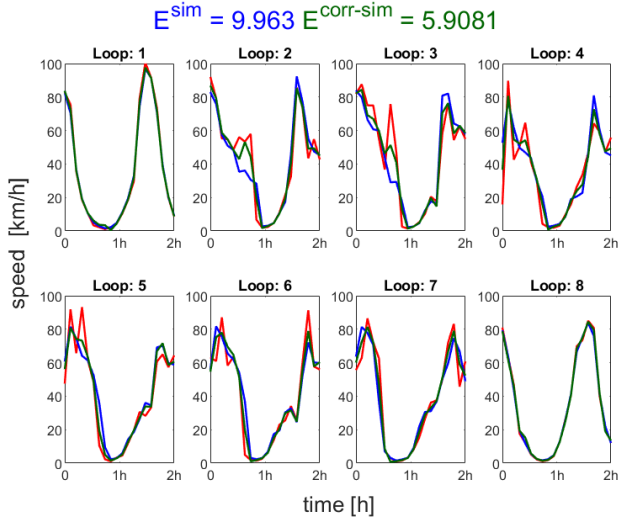


Fig. 6: Speed profiles for GSOM-KOH. In red: field data y^F , in blue: sim. data y^M , in green: corr. sim. data y_c^M .

TABLE II: RMSE between \bar{y}^P and y_c^M .

	τ	LWR	GSOM		τ	LWR	GSOM
L2	0.00	2.44	2.89	KOH	0.00	2.48	3.33
	0.02	4.85	6.65		0.02	4.75	6.62
	0.10	6.29	9.40		0.10	6.11	7.66

model is equipped with more information (speed values for boundary loop detectors), it does not perform better in the speed reconstruction. This result is in contrast with [3], where real traffic data are considered, but on a much shorter road stretch (1.1 km) without any ramps. However, this is instead coherent with what observed in [20], [21].

VI. CONCLUSION

In the synthetic data case including biases, it is not possible to reconstruct the ground truth parameter θ^0 exactly. However, we observed that parameter calibration can lead to a low error \mathbf{E} , which is desirable for the reconstruction of y^F . Moreover, we analyzed the different contributions of a bias term to the generated data, leading to an outperformance of the LWR over the GSOM model. This is visible especially in higher bias situations. In these cases, we observed also that the KOH approach captures better the bias modeling. Thus, if the intention is travel time prediction and if we assume a bias in the data, the LWR-KOH setting seems to be the best candidate. In future works, we will continue by considering real traffic data (such as the RTMC data set [18]). Due to the complexity of real traffic situations, it will be more difficult to obtain a good data reconstruction by numerical simulation. However, this paper can be seen as a benchmark when testing the different calibration approaches on real data.

REFERENCES

[1] S. Fan, M. Herty, and B. Seibold, "Comparative model accuracy of a data-fitted generalized Aw-Rascle-Zhang model," *Netw. Heterog.*

Media, vol. 9, no. 2, pp. 239–268, 2014. [Online]. Available: <https://doi.org/10.3934/nhm.2014.9.239>

[2] G. Dervisoglu, G. Gomes, J. Kwon, R. Horowitz, and P. Varaiya, "Automatic calibration of the fundamental diagram and empirical observations on capacity," in *Transportation Research Board 88th Annual Meeting*, vol. 15. Citeseer, 2009, pp. 31–59.

[3] A. Würth, M. Binois, P. Goatin, and S. Göttlich, "Data-driven uncertainty quantification in macroscopic traffic flow models," *Advances in Computational Mathematics*, vol. 48, no. 6, pp. 1–26, 2022.

[4] D. Ngoduy and S. Hoogendoorn, "An automated calibration procedure for macroscopic traffic flow models," *IFAC Proceedings Volumes*, vol. 36, no. 14, pp. 263–268, 2003, 10th IFAC Symposium on Control in Transportation Systems 2003, Tokyo, Japan, 4–6 August 2003. [Online]. Available: <https://www.sciencedirect.com/science/article/pii/S1474667017324308>

[5] G. Strofylas, K. Porfyri, I. Nikolos, A. Delis, and M. Papageorgiou, "Using synchronous and asynchronous parallel differential evolution for calibrating a second-order traffic flow model," *Advances in Engineering Software*, vol. 125, pp. 1–18, 2018. [Online]. Available: <https://www.sciencedirect.com/science/article/pii/S0965997817308645>

[6] P. Wagner, "Fluid-dynamical and microscopic description of traffic flow: a data-driven comparison," *Philos. Trans. R. Soc. Lond. Ser. A Math. Phys. Eng. Sci.*, vol. 368, no. 1928, pp. 4481–4495, 2010. [Online]. Available: <https://doi.org/10.1098/rsta.2010.0122>

[7] M. C. Kennedy and A. O'Hagan, "Bayesian calibration of computer models," *Journal of the Royal Statistical Society: Series B (Statistical Methodology)*, vol. 63, no. 3, pp. 425–464, 2001.

[8] D. Higdon, M. Kennedy, J. C. Cavendish, J. A. Cafoe, and R. D. Ryne, "Combining field data and computer simulations for calibration and prediction," *SIAM Journal on Scientific Computing*, vol. 26, no. 2, pp. 448–466, 2004.

[9] M. J. Bayarri, J. O. Berger, M. C. Kennedy, A. Kottas, R. Paulo, J. Sacks, J. A. Cafoe, C.-H. Lin, and J. Tu, "Predicting vehicle crashworthiness: Validation of computer models for functional and hierarchical data," *Journal of the American Statistical Association*, vol. 104, no. 487, pp. 929–943, 2009.

[10] M. Plumlee, "Bayesian calibration of inexact computer models," *Journal of the American Statistical Association*, vol. 112, no. 519, pp. 1274–1285, 2017.

[11] J.-P. Lebacque, S. Mammari, and H. Haj-Salem, "Generic second order traffic flow modelling," in *Transportation and Traffic Theory 2007*, 2007.

[12] J.-P. Lebacque, H. Haj-Salem, and S. Mammari, "Second order traffic flow modeling: supply-demand analysis of the inhomogeneous riemann problem and of boundary conditions," *Proceedings of the 10th Euro Working Group on Transportation (EWGT)*, vol. 3, no. 3, 2005.

[13] M. J. Lighthill and G. B. Whitham, "On kinematic waves. II. A theory of traffic flow on long crowded roads," *Proc. Roy. Soc. London Ser. A*, vol. 229, pp. 317–345, 1955. [Online]. Available: <https://doi.org/10.1098/rspa.1955.0089>

[14] P. I. Richards, "Shock waves on the highway," *Operations Res.*, vol. 4, pp. 42–51, 1956. [Online]. Available: <https://doi.org/10.1287/opre.4.1.42>

[15] C. F. Daganzo, "The cell transmission model: A dynamic representation of highway traffic consistent with the hydrodynamic theory," *Transportation Res. Part B*, vol. 28, no. 4, pp. 269–287, 1994.

[16] R. Franklin, "The structure of a traffic shock wave," *Civil Engineering Publ. Wks. Rev.*, vol. 56, pp. 1186–1188, 1961.

[17] G. Newell, "A theory of traffic flow in tunnels," *Theory of Traffic Flow*, pp. 193–206, 1961.

[18] Minnesota Department of Transportation, "Mn/Dot Traffic Data." Website: <http://data.dot.state.mn.us/datatools/>.

[19] M. A. Osborne, "Bayesian gaussian processes for sequential prediction, optimisation and quadrature," Ph.D. dissertation, Oxford University, UK, 2010.

[20] B. Piccoli, K. Han, T. L. Friesz, T. Yao, and J. Tang, "Second-order models and traffic data from mobile sensors," *Transportation Research Part C: Emerging Technologies*, vol. 52, pp. 32–56, 2015. [Online]. Available: <https://www.sciencedirect.com/science/article/pii/S0968090X14003635>

[21] R. Shi, Z. Mo, K. Huang, X. Di, and Q. Du, "A physics-informed deep learning paradigm for traffic state and fundamental diagram estimation," *IEEE Transactions on Intelligent Transportation Systems*, vol. 23, no. 8, pp. 11 688–11 698, 2022.